

Supporting Information

Doubly Resonant Plasmonic Hot Spot-Exciton Coupling Enhances Second Harmonic Generation from Au/ZnO Hybrid Porous Nanosponges

Jue-Min Yi,^{1} Dong Wang,² Felix Schwarz,³ Jinhui Zhong,¹ Abbas Chimeh,¹ Anke Korte,¹
Jinxin Zhan,¹ Peter Schaaf,² Erich Runge,³ and Christoph Lienau^{1,4}*

¹ Institut für Physik and Center of Interface Science, Carl von Ossietzky Universität
Oldenburg, 26129 Oldenburg, Germany.

² Institut für Mikro- und Nanotechnologien MacroNano® and Institut für Werkstofftechnik,
Fachgebiet Werkstoffe der Elektrotechnik, Technische Universität Ilmenau, 98693 Ilmenau,
Germany.

³ Institut für Mikro- und Nanotechnologien MacroNano® and Institut für Physik, Technische
Universität Ilmenau, 98693 Ilmenau, Germany.

⁴Forschungszentrum Neurosensorik, Carl von Ossietzky Universität, 26111 Oldenburg,
Germany.

*juemin.yi@uni-oldenburg.de.

1. Preparation of bare Au and Au/ZnO hybrid nanosponges	S2
2. Electron-diffraction imaging of a ZnO-filled Au nanosponge.....	S2
3. Third-harmonic spectra of bare Au and Au/ZnO hybrid nanosponges.....	S3
4. Incoherent two-photon luminescence from bare Au and Au/ZnO hybrid nanosponges...	S3
5. Spatial map of the nonlinear emission intensity from Au/ZnO hybrid nanosponges	S3
6. Second-harmonic spectra of an ensemble of bare Au and Au/ZnO hybrid nanosponges	S5
7. Simulated second harmonic spectra of bare Au and Au/ZnO hybrid nanosponges.....	S5

1. Preparation of bare Au and Au/ZnO hybrid nanosponges

Bare Au nanosponges were fabricated by solid-state dewetting and dealloying of an Au/Ag (8 nm/20 nm thick) bilayer film on a SiO₂/Si substrate. Au/Ag alloy nanoparticles were formed when the Au/Ag bilayer was annealed at 900 °C for 15 min in argon atmosphere. The samples were then submerged in HNO₃ (65 wt%) solution for dealloying by removal of Ag from the Ag/Au alloy nanoparticles. After that, Au nanosponges were obtained with a quasi-three-dimensional network of ligaments over the entire nanoparticles. The average diameter of the fabricated half-spherical particles is around 400 nm, and the pore size is around 10-20 nm. The Au nanosponges were subsequently transferred onto a conductive indium tin oxide (ITO)-glass substrate.

For the preparation of Au/ZnO hybrid nanosponges, a 10 nm thick ZnO layer was homogeneously deposited inside the porous structure of the as-prepared bare Au nanosponges with plasma-enhanced atomic layer deposition (PE-ALD) at 150 °C. Then, the samples were annealed at 500°C in Ar for 1 h for the crystallization of the ZnO to improve the optical properties.

2. Electron-diffraction imaging of a ZnO-filled Au nanosponge

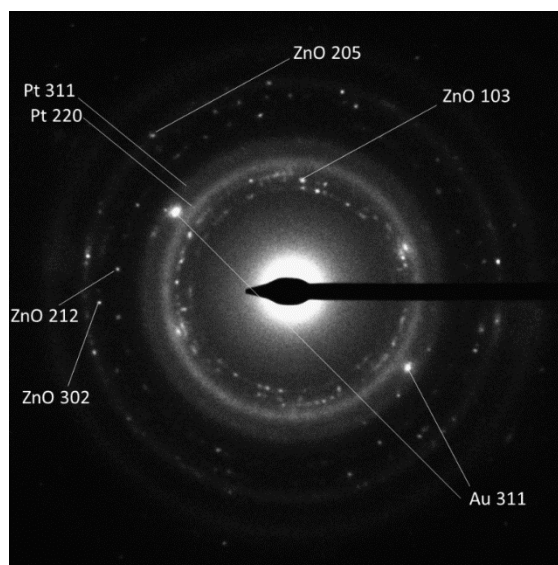


Figure S1. Electron diffraction image taken from a Au/ZnO hybrid nanosponge. Two brilliant points assigned to Au (311) confirm the single crystalline nature of the gold region. The image also shows several dotted rings that can be assigned to the infiltrated ZnO material. They confirm the polycrystalline nature of the infiltrated zinc oxide material. In addition, a polycrystalline platinum layer that has been deposited as a protection layer during the FIB milling can be also identified by the two platinum rings.

In order to check the crystalline structure of both the gold and the zinc oxide regions in the individual hybrid nanosponges, electron diffraction images of selected areas of an individual sponge have been recorded. A representative diffraction pattern is shown in Figure S1. The (311) and (220) rings indicate diffraction by the polycrystalline Pt layer that has been deposited for protection during FIB milling. Two (311) points can be assigned to the gold film, suggesting

that the entire gold scaffold is single crystalline. The polycrystalline structure of the ZnO regions is evident from the observation of several dotted ring structures.

3. Third-harmonic spectra of bare Au and Au/ZnO hybrid nanosponges

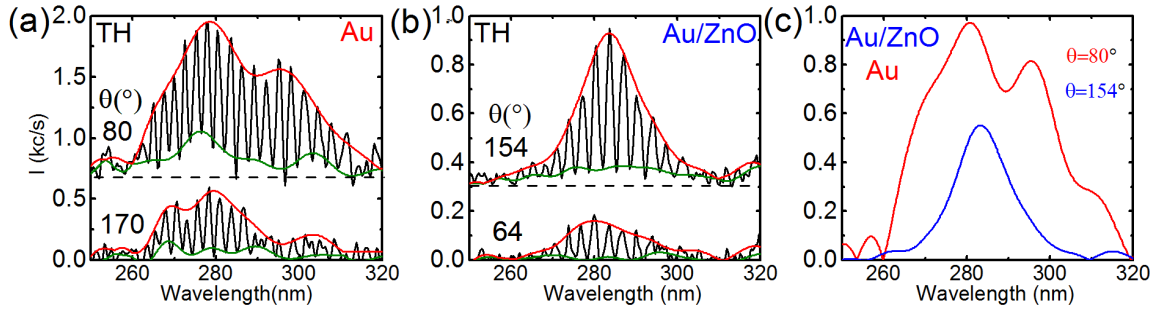


Figure S2. Third-harmonic spectra of a bare Au nanosponge (a) and a Au/ZnO hybrid nanosponge (b) for two incident polarization angles corresponding to the maxima and minima of the spectrally integrated intensities in Figure 2 in the main text. The spectra are vertically shifted (dashed lines) for clarity. (c) The TH spectra from the bare Au are shown at a polarization angle of $\theta = 80^\circ$ and that from the Au/ZnO hybrid nanosponge at $\theta = 154^\circ$, respectively. The maximum TH signal of the Au/ZnO hybrid is reduced by a factor of 1.8, from a peak value of 0.97 kc/s (Au) to 0.54 kc/s (Au/ZnO). The spectrally-integrated TH signal, integrated from 260 nm to 320 nm, from the Au/ZnO hybrid is reduced by a factor of 3.2 with respect to that from the bare Au nanosponge.

4. Incoherent two-photon luminescence from bare Au and Au/ZnO hybrid nanosponges

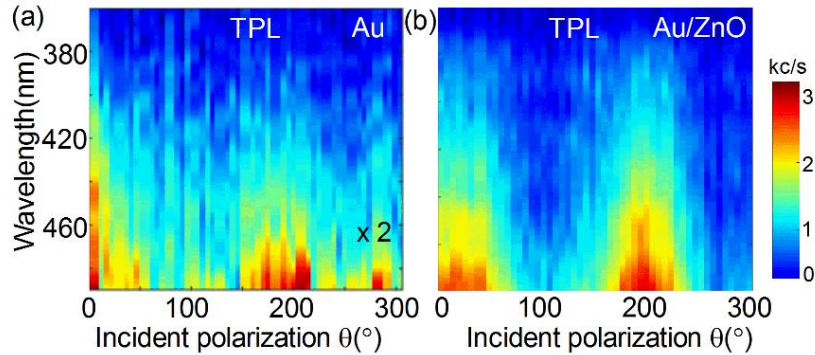


Figure S3. Two-photon photoluminescence (TPL) spectra of (a) a bare Au nanosponge and (b) a Au/ZnO hybrid nanosponge recorded as a function of incident polarization angle θ . The data are extracted from Figure 2 in the main manuscript by Fourier filtering. In both cases, the TPL spectra are similar and red-shifted with respect to the SH emission. Also the polarization dependence is similar and indicates a dipolar polarization response.

5. Spatial map of the nonlinear emission intensity from Au/ZnO hybrid nanosponges

Local nonlinear optical spectra of individual nanosponges are recorded by raster-scanning the samples with dispersed nanosponges through a laser focus and collecting and spectrally dispersing the emitted nonlinear signal in a back-reflection geometry (Figure S4). In this way, spatial maps of the nonlinear emission intensity $I_{\text{NL}}(x, y)$ from different particles are recorded by spectrally integrating the nonlinear spectra at each scanning point. Emission around the 3rd-harmonic (290 nm) of the incident laser is fully dominated by coherent third harmonic emission

while the emission around the 2nd-harmonic (400 nm) includes both second harmonic (SH) generation and two-photon luminescence (TPL). These spectra can further be decomposed into the SH spectrum $I_{\text{SH}}(x, y)$ and TPL spectrum $I_{\text{TPL}}(x, y)$ by filtering the Fourier Transforms of the nonlinear spectra. Figure S4a-b shows the nonlinear intensity maps $I_{\text{NL}}(x, y)$, spectrally integrated between 360 and 480 nm, from several dispersed Au/ZnO hybrid nanosponges (Figure S4c). The data have been recorded for excitation with two orthogonal incident polarizations. Such maps clearly show the polarization dependence of the nonlinear spectra, reflecting the anisotropic properties of the nonlinear signal emitted from the nanosponges.

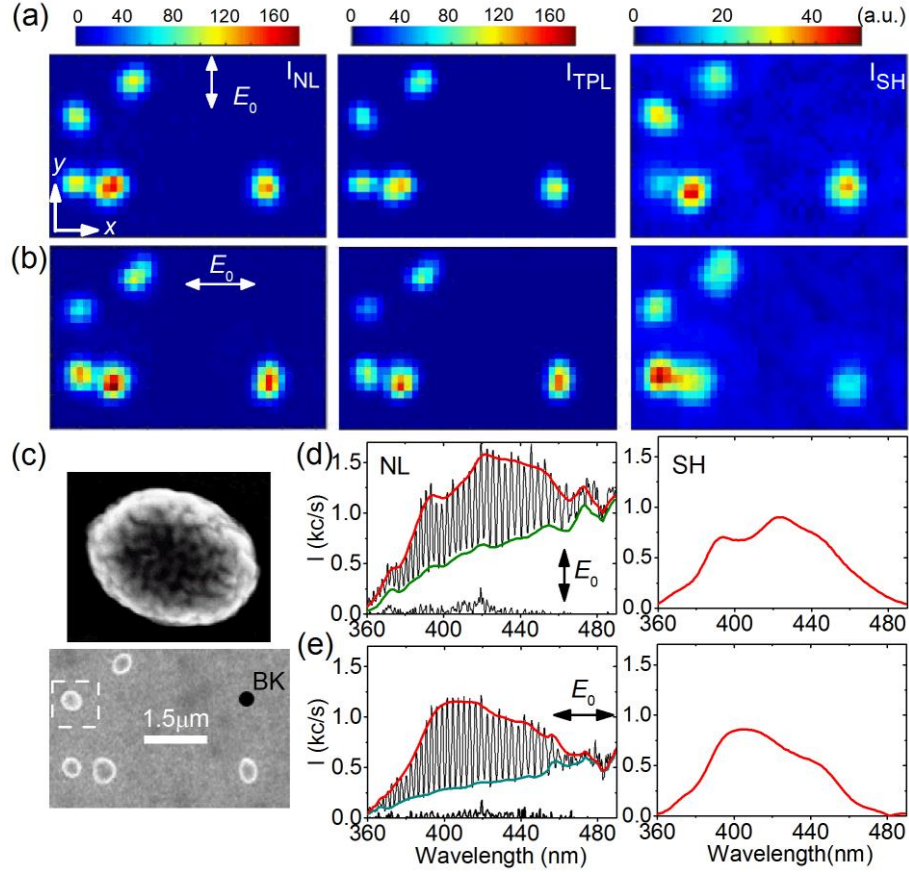


Figure S4. Spatially resolved maps of the nonlinear emission (SH/TPL) from Au/ZnO nanosponges, spectrally integrated between 360 and 480 nm for (a) vertically and (b) horizontally polarized excitation. The TPL (middle panel) and SH (right panel) are separated by Fourier filtering. (c) SEM image of hybrid nanosponges dispersed on a glass surface, and a zoomed image of a single nanosponge (marked with dashed lines). (d) and (e) Nonlinear spectra recorded with pulse-pair excitation with an interpulse time delay τ of 200 fs for two orthogonal incident polarizations. Coherent SH is clearly distinguished from an incoherent TPL background. The nonlinear spectra recorded from the 10-nm thick ZnO layer at a reference position ‘BK’ show no measurable signal. Right: Corresponding SH spectra of hybrid sponges, extracted by Fourier filtering.

Figure S4d-e depict the nonlinear spectra from a hybrid nanosponge and 10-nm thick ZnO layer, recorded for horizontally and vertically polarized incident light, respectively. Note that the nonlinear emission from the thin ZnO layer is so much weaker that it can fully be neglected. The extracted SH spectra $I(\lambda)$ from the hybrid nanosponge are depicted as well. Their

amplitude A , center wavelength λ_c and linewidth $\Delta\lambda$ are calculated as $A = \max[I(\lambda)]$, $\lambda_c = \int I(\lambda) \cdot \lambda d\lambda / \int I(\lambda) d\lambda$ and $\Delta\lambda = 2\sqrt{2\ln 2} \cdot \left(\sqrt{\int I(\lambda) \cdot (\lambda - \lambda_c)^2 d\lambda} / \int I(\lambda) d\lambda \right)$.

6. Second-harmonic spectra of an ensemble of bare Au and Au/ZnO hybrid nanosponges

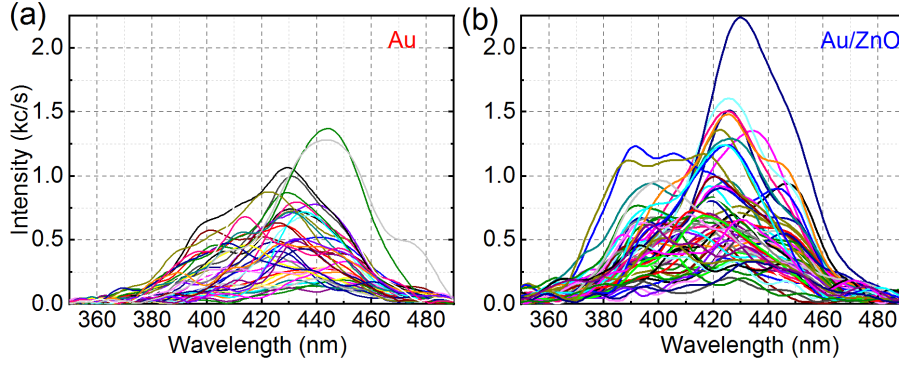


Figure S5. SH spectra of the ensemble of bare and ZnO-functionalized Au nanosponges analyzed in Figure 5 of the main manuscript. The data have been recorded with linearly polarized light with fixed incident polarization direction. Since the SH enhancement near the ZnO bandgap in the hybrid sponges depends sensitively on the incident polarization, only some of the sponges show a clear SH enhancement around 390 nm.

7. Simulated second harmonic spectra of bare Au and Au/ZnO hybrid nanosponges

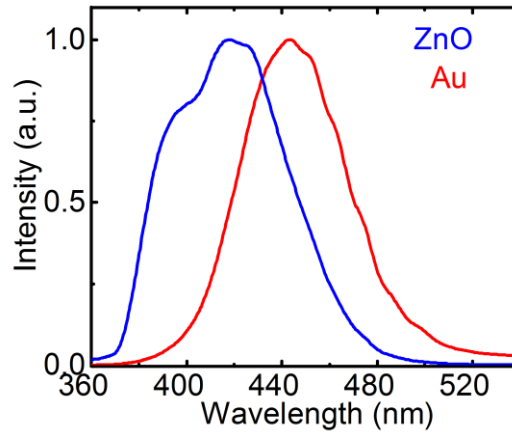


Figure S6. Simulated spectra of the second harmonic emission from gold, $|P_{\text{Au}}^{(2)}(\lambda)|^2$, and from ZnO, $|P_{\text{ZnO}}(\lambda)|^2$, for the Au/ZnO hybrid nanosponge. The two components are obtained from Eq. (1) and Eq. (2) in main text, respectively. The simulation parameters have been chosen to match the ensemble-averaged SH emission spectrum of the hybrid nanosponge shown in Figure 6 of the main text.